

Ultrallicky/hydrophilic patterned surfaces for efficient fog harvest

Biao Qi^a, Xiaolong Yang^{a,b,*}, Xiaolei Wang^a

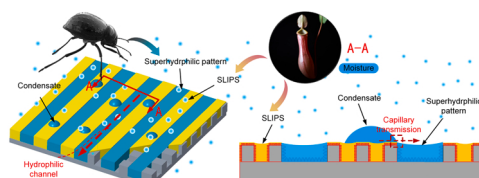
^a College of Mechanical and Electrical Engineering, Nanjing University of Aeronautics and Astronautics, Nanjing 210016, PR China

^b Jiangsu Key Laboratory of Precision and Micro-Manufacturing Technology, Nanjing University of Aeronautics and Astronautics, Nanjing 210016, PR China

HIGHLIGHTS

- Hydrophilic patterns were fabricated on hydrophobic surfaces by laser processing.
- This laser processing method is suitable for many substrates.
- Hydrophilic patterned slippery surfaces showed excellent droplet anisotropy.
- Hydrophilic patterned slippery surfaces showed excellent fog harvest performance.

GRAPHICAL ABSTRACT



ARTICLE INFO

Keywords:

Slippery surface
Droplet transport
Fog harvest
Superhydrophobic surface
Hydrophilic pattern

ABSTRACT

The rapid and controllable sliding of droplets on anisotropic slippery liquid infused porous surfaces (SLIPS) has promising application prospects in the fields of energy, lab-on-a-chip, etc. In this work, the fabrication of hydrophilic patterned SLIPS on copper substrates that can achieve efficient droplet transport and fog harvest was reported. A single superhydrophilic stripe and array of superhydrophilic stripes were fabricated on SLIPS background, respectively. Contact angles, sliding angles and contact angle hysteresis of the surfaces were investigated and analyzed. Results showed that hydrophilic patterned SLIPS with superhydrophilic stripe array had remarkable anisotropy in contact angle hysteresis in the parallel and perpendicular directions due to the large energy barrier induced by liquid surface tension in the direction perpendicular to the stripes, which can be used to transport droplets rapidly and precisely. In addition, the fog harvest performance, as a typical example of droplet transport, was significantly improved on hydrophilic patterned SLIPS due to high nucleation density on the hydrophilic SLIPS, high condensate mobility, efficient condensate transferring from SLIPS to superhydrophilic stripes and liquid shedding along the stripes for departing.

1. Introduction

Superhydrophobic surfaces (with water contact angle $> 150^\circ$) play critical roles in a wide range of engineering applications, such as self-cleaning, anti-icing, drag reduction, oil-water separation due to ultra-low affinity toward water.[1–7] In addition, droplet manipulations, such as droplet storage, transport and mixing, which have been intensively used in microfluidic devices,[8] high-throughput cell screening,[9] etc., as well as their recently developed application in water harvest,[10]

were readily achievable by introducing either external field (magnetism, electrostatic field, light and thermal)[11–13] or high adhesion hydrophilic/hydrophobic patterns on superhydrophobic background.[14–18] For instance, An et al. realized effective control of both static droplets and mobile droplets for their transport in multi-channel systems by light source.[13] Shiratori et al. used techniques based on complete hydrophobicity to design both dynamic and static hydrophobic/hydrophilic patterned surfaces to control the direction of droplet movement.[15] Hou et al. fabricated superhydrophilic triangle patterns on

* Corresponding author at: College of Mechanical and Electrical Engineering, Nanjing University of Aeronautics and Astronautics, Nanjing 210016, PR China.

E-mail address: xlyang@nuaa.edu.cn (X. Yang).

<https://doi.org/10.1016/j.colsurfa.2022.128398>

Received 10 November 2021; Received in revised form 18 January 2022; Accepted 21 January 2022

Available online 25 January 2022

0927-7757/© 2022 Elsevier B.V. All rights reserved.

superhydrophobic surfaces via laser ablation, thus facilitating the transport of condensate.[16] However, superhydrophobic surfaces that function based on air cushions trapped in micro/nano structures tended to be damaged in harsh working conditions, especially in the application of water harvesting where fog condensed and grew within the micro/nano structure, leading to complete flooding.[19–21] Inspired by the *Nepenthes* pitcher, slippery liquid-infused porous surfaces (SLIPS) with ultra-low contact angle hysteresis, self-healing, and pressure stability have been widely studied.[22] Droplets on the SLIPS infused with lubricant moved easily due to the ultralow sliding resistance at the droplet-lubricant interface and were hard to penetrate into the structures beneath the lubricant to damage the surface. The robust SLIPS enlightened various applications from water collection, self-cleaning, corrosion protection to anti-icing.[23–30] For instance, Wang et al. fabricated SLIPS on zinc surfaces with the hydrothermal method and found that the SLIPS exhibited better corrosion resistance compared with superhydrophobic surfaces.[28] On homogeneous SLIPS, sliding resistance in all directions along the surface was low and consistent, namely, droplet movement was easy to initiate but it was hard to control the sliding direction.[31] Directional motion of droplets on SLIPS can be achieved by controlling the topology of the droplet-lubricant interface.[32–38] For instance, inspired by the beetle's bumpy surface geometry in enhancing condensation, Park et al. designed surfaces covered with slippery asymmetric bumps; condensate droplets can be transported on the fabricated SLIPS against gravity due to the capillary force.[33] Ling et al. proposed a method using an inkjet printer to define slippery patterns to fabricate the bowl-like SLIPS on poly (dimethylsiloxane) (PDMS) substrates, the patterned slippery surface can be employed as a microfluidic device to guide, transport and mix droplets.[34] In addition to topological SLIPS that activated directional droplet movement via control of droplet footprint, SLIPS with patterns with different wettability (superhydrophilic patterns) are good candidates as the superhydrophilic patterns have strong anisotropic adhesion while the SLIPS background is robust enough to resist the droplet pinning for long-term operation in harsh applications, for example, fog harvest. A few notable studies succeeded in the fabrication of hydrophilic patterned SLIPS for droplet motion control and water collection.[39,40] However, the chemical methods used in these studies were complex and limited to a few materials. Hence, the development of simple and universal methods for creating stable hydrophilic patterned SLIPS with excellent droplet manipulation ability still attracts considerable interest.

In this work, a high-efficient, low cost and easy-implemented technique, laser ablation, was proposed to fabricate hydrophilic patterned SLIPS on copper substrates for fog harvest by combining the slippery property of the peristome of *Nepenthes* and hydrophilic patches inspired by Desert beetle. The thermal conductivity of copper is ~ 397 W/m·K, which is very high and makes copper one of the most important materials for heat transfer devices. The fog harvest is conducted via phase change (condensation), which is highly dependent of thermal conductivity of substrate materials. High thermal conductivity manifests high heat transfer and thereby improved fog harvest rate. Both the wettability stability and droplet motion behavior on the surfaces were investigated before demonstrating a potential application for fog harvest. Results showed that the hydrophilic patterned SLIPS were capable of precisely guiding water movement, and were suitable for efficiently transferring and draining collected water during fog harvest. The droplet manipulation and demonstrated enhanced fog harvest on the biomimetic surface may provide a reference for developing new facilities for water collection, such as fog harvest and desalination.

2. Materials and methods

2.1. Materials

Copper sheets (40 mm × 40 mm × 2 mm) were purchased from Suzhou Metal Material Manufacturer (China). Fluoroalkylsilane [FAS,

$C_8F_{13}H_4Si(OCH_2CH_3)_3$] and hydroxy-terminated polydimethylsiloxane (HTPDMS, viscosity of 40 cst at 25 °C) were purchased from Macklin Co., Ltd (China). Silicon oil (viscosity of 20 cst at 25 °C) was obtained from Dow Corning Co. Ltd. Krytox 1525 (viscosity of 250 cst at 25 °C) and Fomblin Y25/6 (viscosity of 276 cst at 25 °C) were obtained from Sigma-Aldrich. All chemicals were analytically pure and were used as received.

2.2. Fabrication of homogeneous nanotextured SLIPS

Polished copper sheets were first ablated using a UV laser marking machine (KY-M-UV3L, Wuhan Keyi, China) with an average output power of 2.0 W, power intensity of 3.9 J·cm⁻², high scanning rate of 1500 mm·s⁻¹. The ablated sample was then ultrasonically cleaned in 95 wt% ethanol for 3 min to remove excess deposits before being immersed in 1 wt% ethanol solution with fluoroalkylsilane [FAS, $C_8F_{13}H_4Si(OCH_2CH_3)_3$] for 90 min to lower the surface energy and dried at 120 °C for 30 min. Homogeneous SLIPS were obtained by infusing lubricant and rinsing under running water to remove the excess lubricant. The thickness of the lubricant can be controlled by varying the rinsing time. The quality of the remaining lubricant on the surface was measured by a precision electronic balance (JB5374–91, Mettler Toledo, Shanghai), and the thickness was calculated assuming the lubricant was uniform.

2.3. Fabrication of hydrophilic patterned SLIPS

Superhydrophilic patterns were fabricated on the prepared superhydrophobic background using a UV laser marking machine (KY-M-UV3L, Wuhan Keyi). The power of 2.0 W and the laser speed of 1000 mm·s⁻¹ were held constant during the process. After the hydrophilic patterns were patched, the hydrophilic patterned SLIPS were obtained after infusing lubricant followed by fully rinsing under running water to remove excess lubricant and to retain essential water on the superhydrophilic patterns. Infusing and rinsing steps should be switched to some lubricants that have higher affinity for the substrates such as Krytox 1525 and Fomblin Y25/6.

2.4. Fog harvest

A chamber with controlled temperature and humidity was designed to test the fog harvest performance. Ultrasonic humidifiers were used to generate water mist and the humidity in the chamber was controlled by a humidity sensor. A Peltier cooling plate was fixed on the bracket in the chamber and the temperature of the sample placed vertically on the cooling plate was controlled by a temperature sensor. When the sample temperature was lower than the water mist temperature, condensation occurred on the surface of the sample and the condensate was collected by the container directly below the sample. The weight of the container before and after collection was measured by a high-resolution analytical balance (ME204E, Mettler-Toledo Inc., Switzerland), and the difference between the two weights was the mass of the harvested fog. Therefore, the fog harvest rate (Mf) can be calculated as:

$$Mf = M/tS \quad (1)$$

where M is weight of fog harvest, t is the collection time and S is surface area of the sample.

2.5. Characterization

The micro morphology of as-prepared surfaces was analysed using a scanning electron microscope (SEM, Ultra60, Zeiss, Germany) and a digital microscope (VHX-600, Keyence, Japan). Static contact angles and contact angle hysteresis were characterized with a goniometer (Rame-Hart 290, USA). Elements of the surface were characterized with energy-dispersive spectroscopy (EDS, Ultim Max). Images and videos of

droplet motion on the SLIPS were taken by a digital camera with 1000 fps high-speed recording function (RX100M5, Sony, Japan). The mass of the remaining lubricant was measured with a precision electronic balance (JB5374-91, Mettler Toledo, Shanghai).

3. Results and discussion

3.1. Construction of hydrophilic patterned SLIPS

Inspired by the water harvesting strategy of Desert beetles and slippery peristome of *Nepenthes* pitcher plants (Fig. 1a), hydrophilic patterned SLIPS consisting of *Nepenthes*-like SLIPS background and Desert beetle-like superhydrophilic stripe patterns were designed and fabricated via laser ablation for creating microstructures on copper substrates, FAS modification for acquiring superhydrophobicity, second laser ablation for patching superhydrophilic patterns and finally infusing lubricant for finally obtaining the surface (Fig. 1b). On the surface, high dense condensate nucleated on the SLIPS was transferred to the superhydrophilic patterns due to the Laplace pressure difference for converging and draining away with the aid of gravity once contacting the pattern. (Fig. 1c).

As shown in Fig. 2a, dense hierarchical papilla microstructures with nano villus, which were crucial for superwetting, were produced on the copper substrates by taking advantage of phase explosion, melting and resolidification during laser ablation. Fig. S1 shows the schematic diagram of the nanosecond pulse laser scanning in the experiment. The morphology of the grooves in the scanning area in Fig. 2a was created by the resolidification and accumulation of the molten material.[41] After surface modification in 1 wt% FAS (fluoroalkylsilane) ethanol solution, elements of C, Si and F were detected, which demonstrated that Si-O-Si and C-F groups with low surface energy were successfully assembled on the surface. A 5 μ L water droplet dispensed on such a surface had a

contact angle of $\sim 161^\circ$ and a sliding angle of $\sim 2.5^\circ$, displaying excellent static and dynamic superhydrophobicity.

To patch superhydrophilic patterns on the superhydrophobic background, the dependence of the output laser power and scanning rate on the wettability of laser ablated area was investigated (Fig. S2). When output laser power was set as 2.0 W and scanning rate was $1000 \text{ mm}\cdot\text{s}^{-1}$, superhydrophobicity of the surface was completely erased, reaching a superhydrophilic state with contact angle close to 0° . SEM images of the ablated superhydrophilic patterns presented hierarchical microstructures similar to the superhydrophobic surfaces. However, elements of Si and F, which represent the low surface energy groups of Si-O-Si and C-F in the superhydrophilic region were greatly reduced in EDS spectrum (Fig. 2b). Superhydrophilic patterns with different shapes were easy to fabricate by designing scanning path of laser using mapping software. Finally, the hydrophilic patterned SLIPS (SLIPS with superhydrophilic patterns) were obtained after infusing lubricant followed by fully rinsing under running water to remove excess lubricant and retain essential water on the superhydrophilic patterns. Infusing and rinsing steps should be switched to some lubricants that have higher affinity for the substrates.

3.2. Droplet behavior on hydrophilic patterned SLIPS

The physicochemical properties (viscosity and surface tension) of lubricants affected the viscous force between water and lubricant, determined whether the droplet was cloaked and the sliding resistance. As a result, the lubricant should be selected carefully before creating the hydrophilic patterned SLIPS. Four different lubricants including hydroxy-terminated polydimethylsiloxane (HTPDMS), silicone oil (PDMS), Krytox 1525 and Fomblin Y25/6 were used to infuse the superhydrophobic surface with a single superhydrophilic stripe pattern to create single stripe patterned SLIPS (Table S1). Water droplets

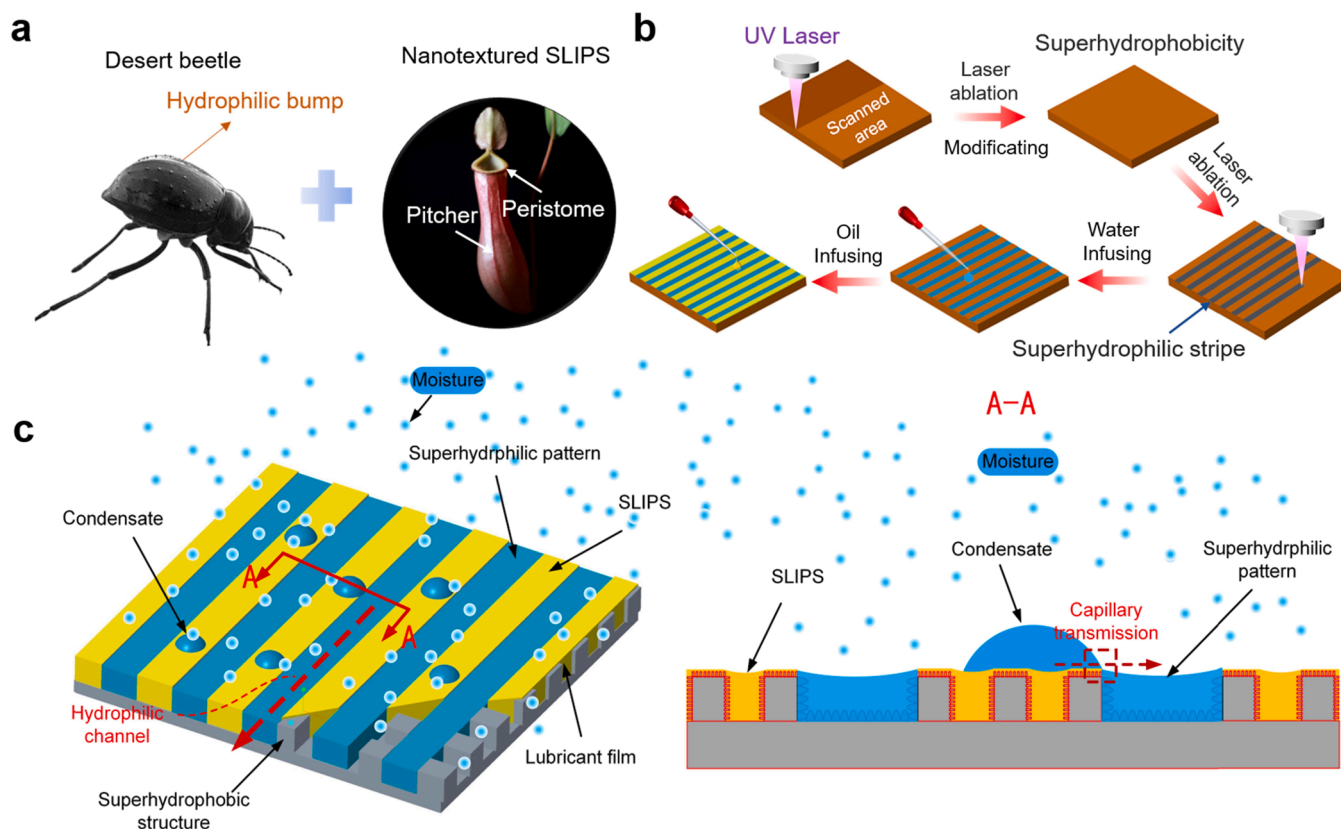


Fig. 1. Construction of hydrophilic patterned SLIPS: (a) A Desert beetle with hydrophilic bumps on its back and a *Nepenthes* pitcher plant with slippery peristome. (b) Processing method of hydrophilic patterned SLIPS. (c) Condensation process of moisture on hydrophilic patterned SLIPS.

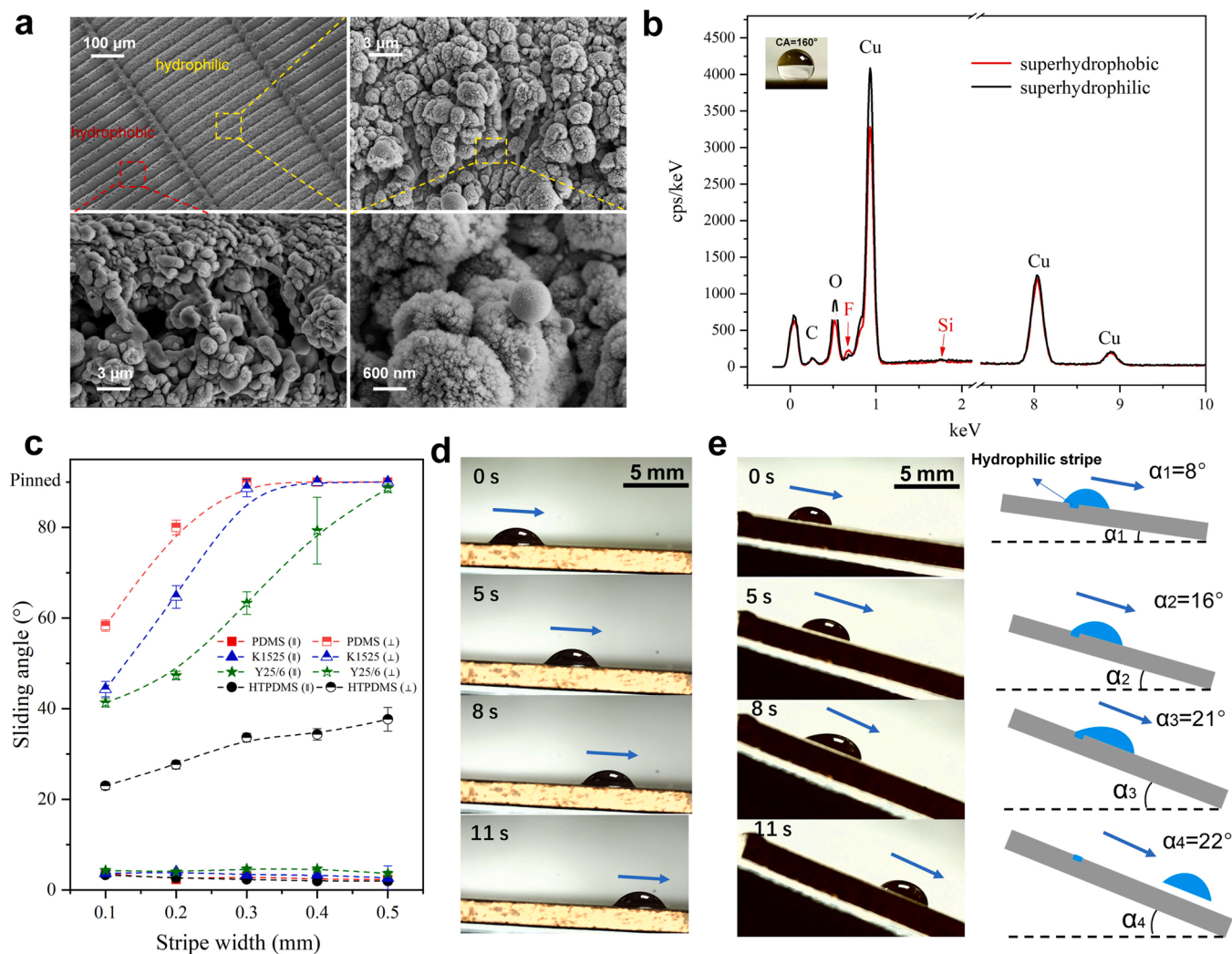


Fig. 2. Droplet behavior on SLIPS with single superhydrophilic stripe: (a) SEM images of superhydrophobic and superhydrophilic regions before lubricant infusing. (b) EDS spectra of superhydrophobic and superhydrophilic regions. (c) Parallel and perpendicular sliding angles of a 10 μL droplet on single superhydrophilic stripe with different widths patterned on SLIPS infused with different lubricants. (d) Time-lapse series photos of a 10 μL droplet sliding in the parallel direction to the hydrophilic. (e) Time-lapse series photos of a 10 μL droplet sliding in the perpendicular direction to the hydrophilic and their corresponding schematic diagram.

dispensed on the stripe showed excellent sliding anisotropy (Fig. 2c). For example, the parallel sliding angle ($SA_{||}$) and perpendicular angle (SA_{\perp}) of a 10 μL water droplet on a 0.1 mm wide stripe patterned on HTPDMS infused SLIPS were 3.2° and 24°, respectively (Fig. 2d, Fig. 2e and Movie S1). The interface of the droplet on the stripe pattern was composite, consisting of a droplet-pattern interface and a droplet-lubricant interface. The droplet needed to overcome viscous force at the droplet-water interface on the stripe and at the droplet-lubricant interface on the surrounding SLIPS when the droplet slid along the stripe. The viscous force could be ignored due to the low sliding velocity, which made it easy for the droplet to slide along the stripe. However, the droplet must break the droplet-water interfacial surface tension from the stripe, which is much larger than the viscous force, to slide in the direction perpendicular to the stripe. Different degrees of SA anisotropy were achievable by changing the type of lubricant or stripe width. For the same lubricant, by increasing the width of the pattern, the SA_{\perp} increased until a pinning state occurred while the $SA_{||}$ remained a very low level. For different lubricants, experimental measurements showed that the sliding anisotropy of the droplet increased mainly as the surface tension of the lubricant decreased, because the droplet needed to overcome the higher energy barrier caused by the increased wetting gradient. In addition, the motion of droplets on the superhydrophilic stripes with

different depths was studied, and results demonstrated that depth had little effect on sliding anisotropy (Fig. S3).

The above results showed that SLIPS with a single superhydrophilic stripe had excellent sliding anisotropy, which could be used to efficiently guide droplet transport. On the basis of the above analysis, SLIPS with array of superhydrophilic stripes were created to enhance the sliding anisotropy. Stripe arrays with widths of 0.3 mm, 0.4 mm and 0.5 mm, respectively, were fabricated on SLIPS infused with four types of lubricants. The stripe spacing was set to be equal to the width. Fig. 3a presented the elongated shape of a 20 μL droplet dispensed on the SLIPS with 0.5 mm wide superhydrophilic stripes, which manifested that droplet tended to spread along the stripe due to the capillary force and to be confined perpendicularly due to the energy barrier induced by the stripes. The parallel contact angle ($CA_{||}$) and perpendicular contact angle (CA_{\perp}) of the droplet on the surface were 37° and 55°, respectively, indicating obvious static contact angle anisotropy (Fig. 3b and Fig. 3c). Fig. 3d and Fig. 3e described the $CA_{||}$ and CA_{\perp} versus stripe widths and spacings. Results showed that contact angles trended to increase with the decrease of stripe spacing.

The $SA_{||}$ and SA_{\perp} on hydrophilic patterned SLIPS with superhydrophilic stripe array also showed obvious anisotropy (Fig. 3f and Fig. 3g). The experimental results showed that the sliding anisotropy

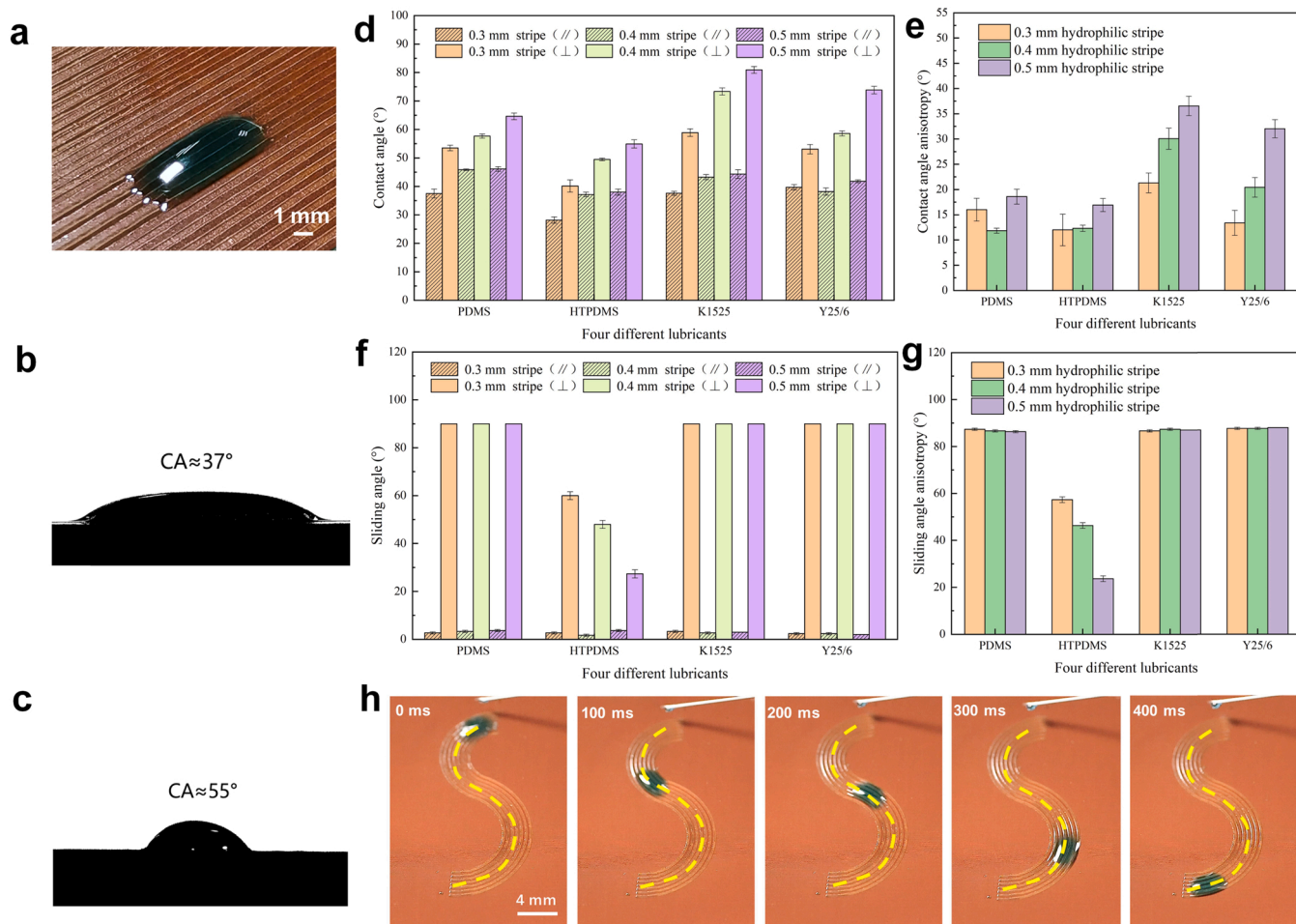


Fig. 3. Droplet behavior on SLIPS with array of superhydrophilic stripes: (a) A droplet on the SLIPS with superhydrophilic stripes. (b) Image of the droplet in parallel direction. (c) Image of the droplet in perpendicular direction. (d) The parallel and perpendicular CAs and (f) SAs of 10 μL droplets on array of superhydrophilic stripes with different widths (The stripe width was the same as the stripe spacing and four different lubricants were used). (e) Contact angle and (g) sliding angle anisotropy of droplets. (h) Time-lapse photos of transporting a 10 μL droplet on SLIPS with array of S-shaped stripes (the widths and spacings of the stripes were both 0.3 mm, and the surface was infused with PDMS).

was related to the width and spacing of the stripe and the type of lubricant. When low surface tension lubricants such as PDMS, Y25/6, and K1525 were used, the width and spacing of the stripes had little effect on the sliding anisotropy, the droplet could reach a pinning state in the perpendicular direction while SA_{\parallel} remained a very low level for all stripe widths ranging from 0.3 to 0.5 mm. For the surfaces infused with HTPDMS, the energy barrier that the droplet had to overcome for move in the perpendicular direction became smaller because the wetting gradient between the superhydrophilic region and the SLIPS region decreased. As a result, the sliding anisotropy was relatively low and was obviously related to the widths and spacings of the stripes. The sliding anisotropy of the droplet tended to increase with the decrease of the spacing and width because the increasing number of hydrophilic stripes led to greater sliding resistance to the droplet.

In order to demonstrate the feasibility of transporting droplets using the hydrophilic patterned SLIPS, SLIPS patterned with array of S-shaped stripes with a width and spacing of 0.3 mm were fabricated to transport a 10 μL droplet. As shown in Fig. 3h, the 10 μL droplet released from the syringe precisely moved along the S-shaped stripes with the aid of gravity at an average velocity of 100 $\text{mm}\cdot\text{s}^{-1}$ (Movie S2).

The sliding resistance F_{re} for droplets sliding on a surface can be calculated using the following equilibrium formula:[42–44].

$$F_{\text{re}} = \rho g V s \sin \alpha \quad (2)$$

where ρ is the density of the droplet ($\text{g}\cdot\text{cm}^{-3}$), g is the gravitational acceleration, V is the volume of the droplet, and α is the sliding angle of the droplet.

In order to better explain the mechanism of sliding anisotropy on the hydrophilic patterned SLIPS, a classic sliding resistance model (Furmidge equation) was adopted to analyze the sliding resistance:

$$F_{\text{re}} = \gamma \cdot W_{\text{dp}} (\cos \theta_{\text{R}} - \cos \theta_{\text{A}}) \quad (3)$$

where γ is the surface tension between the droplet and the surrounding medium, W_{dp} is the width of the droplet interface perpendicular to the sliding direction, θ_{A} and θ_{R} are advancing and receding contact angle, respectively.

It can be concluded from the above equation that W_{dp} and contact angle hysteresis (defined as the difference between advancing and receding contact angle) dominate the sliding resistance. As a result, advancing and receding contact angles in directions perpendicular and parallel to the stripes of different samples were measured and compared (Fig. 4a and Fig. 4b). Results showed that the contact angle hysteresis in the perpendicular direction was much larger than that in the parallel direction. Meanwhile, the picture of the droplet showed that the length of the droplet in the perpendicular direction is smaller than that in the parallel direction. In the perpendicular direction, the increase in W_{dp} and the contact angle hysteresis leads to an increase in the sliding resistance of the droplets, which requires an increase in the gravity

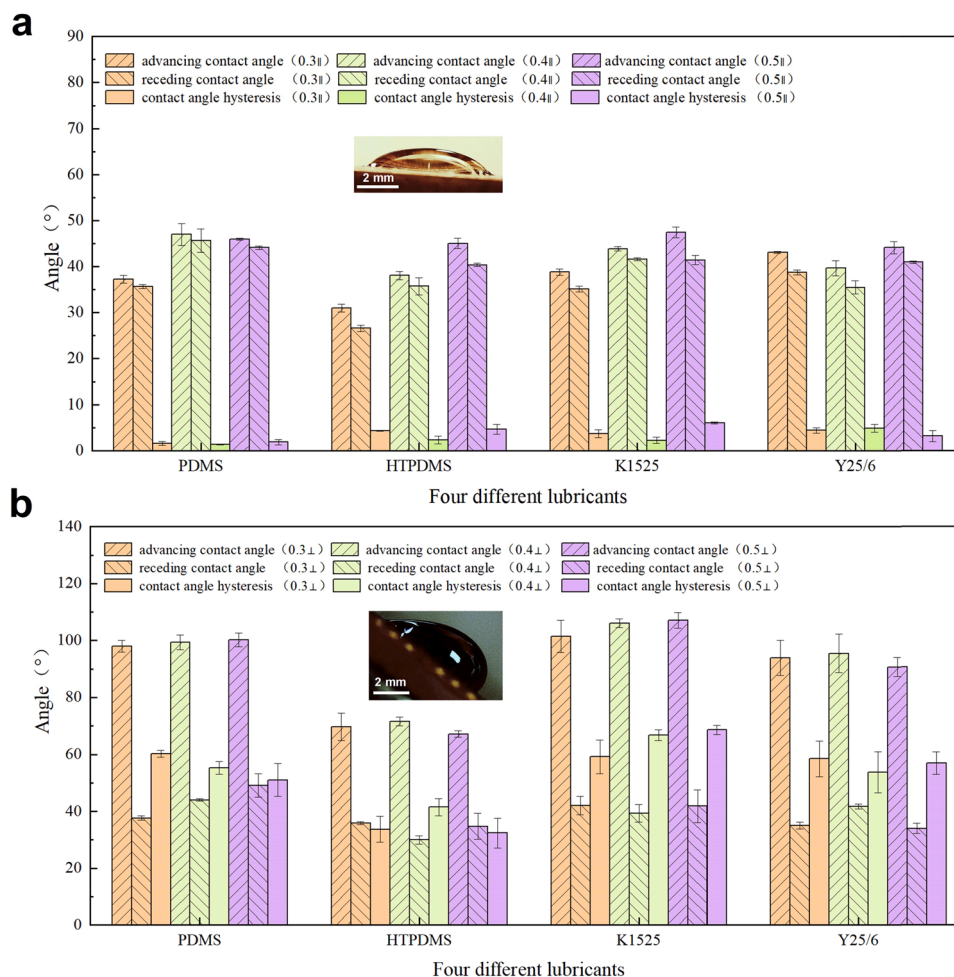


Fig. 4. Advancing angles, receding angles and contact angle hysteresis (a) in parallel direction and (b) in perpendicular direction.

component to overcome the adhesion resistance, thus the SA_{\perp} is much larger than SA_{\parallel} . In addition, the type of lubricant significantly affects the contact angle hysteresis. For HTPDMS with high surface tension, as the wetting gradient decreases, the contact angle hysteresis of the droplet also decreases, which leads to that the anisotropy of the droplet in two directions is not particularly significant. In contrast, the width and spacing of the superhydrophilic stripes have little impact on the contact angle hysteresis of the droplet. Therefore, for droplet motion control, the selection of lubricant should take precedence over the stripe array design.

3.3. Fog harvest

Fog harvest is the foundation of water collection systems, power generation, thermal management, desalination and other energy applications.[45–49] For fog harvest, droplet transport on the surface is critical for condensing droplets for rapid removal. However, at present, there are few functional surfaces that are suitable for harsh working conditions and have excellent fog harvest performance. The hydrophilic patterned SLIPS designed in this work exhibited excellent droplet nucleation and removal ability, as well as high durability when working in harsh environments, thus having great potential in fog harvest.

The fog harvest performances of several bio-inspired surfaces including superhydrophobic surfaces (SHOS), homogeneous SLIPS and hydrophilic patterned SLIPS with superhydrophilic stripe array were investigated. In order to study the effect of the arrangement of superhydrophilic stripes on the fog harvest rate, superhydrophilic stripes with spacing of 0.3 mm, 0.6 mm, 0.9 mm and 1.2 mm were designed and

fabricated on SLIPS background, on which the width of the superhydrophilic stripes was fixed at 0.3 mm. Those samples were denoted for simplicity as SSP0.3, SSP0.6, SSP0.9 and SSP1.2, respectively. In addition, the physicochemical properties (viscosity and surface tension) of lubricants also affect the rate and durability of fog harvest. Therefore, the hydrophobic lubricant Y25/6 ($\theta = 108^{\circ}$) and the hydrophilic lubricant HTPDMS ($\theta = 80^{\circ}$) with lower viscosity were used to create homogeneous SLIPS and hydrophilic patterned SLIPS with superhydrophilic stripe array for the fog collection experiment. Meanwhile, in order to eliminate the influence of lubricant thickness on the condensation performance, the thickness of the lubricant retained on all samples was controlled at about 10 μm (Fig. S4). The prepared samples were attached on the cooling plate in the designed experimental chamber. The temperature of the sample was set to $10 \pm 1^{\circ}\text{C}$. The humidity in the sealed chamber was set to $70 \pm 1\%$ and the temperature in the chamber was $30 \pm 1^{\circ}\text{C}$. Fig. 5a and Fig. 5b showed the fog harvest rate of several different surfaces infused with hydrophilic and hydrophobic lubricants, respectively.

On the superhydrophobic surface, dropwise condensation could be observed (Fig. 5c and Movie S3). When the condensate grew to a certain size, they merged into big droplets. In the process of merging, the surface energy of the droplets was converted into kinetic energy that finally drove droplets to jump off the surface, a phenomenon known as the jumping droplet phenomenon. However, the results showed that the condensation efficiency on superhydrophobic surfaces was relatively lower than that on SLIPS. Three assumptions are as follows: (1) low contact angle of SLIPS represents a large footprint, which means a large effective area for heat transfer and is beneficial for high density

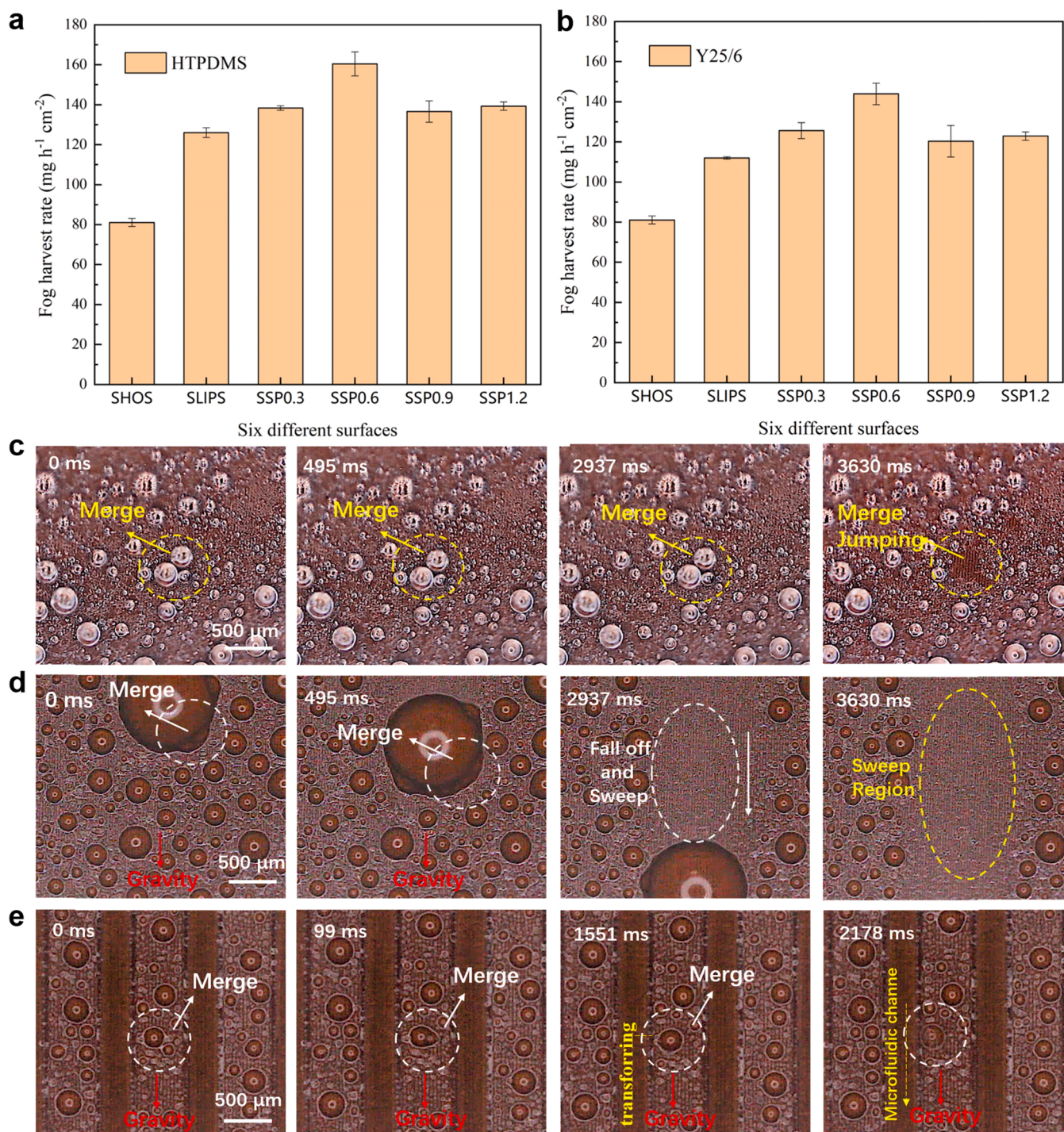


Fig. 5. Fog harvest on superhydrophobic surfaces (SHOS), SLIPS and hydrophilic patterned SLIPS: (a) Fog harvest rates on different surfaces (hydrophilic SLIPS infused with HTPDMS). (b) Fog harvest rates on different surfaces (hydrophobic SLIPS infused with Y25/6). (c) The jumping phenomenon of condensate droplets on superhydrophobic surface. (d) Falling phenomenon of condensate droplets on hydrophilic SLIPS. (e) Merging, transferring and transporting of droplets on the SLIPS with arrays of superhydrophilic stripes. (During the test, all samples were placed vertically).

nucleation; (2) the low sliding resistance of SLIPS facilitates the movement of condensate and improves the ability of condensate drainage; (3) the homogeneous lubricant prohibits the nucleation in the microstructures underneath the lubricant, which avoid the flooding.

On the homogeneous SLIPS, once small condensate came into contact with each other, they would merge into large droplets. When the large droplets grew to a certain size, they would slide off the surface with the aid of gravity and sweep off the small droplets in their falling paths. The surface was thereby renewed and the next cycle of the condensation

process was repeated (Fig. 5d and Movie S4). In addition, results indicated that the fog harvest performance of hydrophilic SLIPS was better than that of hydrophobic SLIPS (Fig. 5a and Fig. 5b), which verified the assumption (1).[19] However, hydrophilic SLIPS still suffered from relatively low condensate drainage efficiency despite the fact that the condensate departing resistance was smaller than that on superhydrophobic surfaces.

On the hydrophilic patterned SLIPS with superhydrophilic stripes, dropwise condensation occurred on the SLIPS areas, while filmwise

condensation occurred on the superhydrophilic stripe region. When the condensate on the SLIPS areas merged and grew to reach the boundary of the superhydrophilic stripe region, they would be transferred to the stripe due to capillary force, and the condensate would be transported along the stripe with the aid of gravity to the tail end for finally departing (Fig. 5e and Movie S5). Compared with homogeneous SLIPS, the superhydrophilic stripe was more conducive for condensate to quickly depart from the surface, thus improving the efficiency of fog harvest on the surface. In addition, the SLIPS with superhydrophilic stripes was robust and could sustain condensation for more than six hours (Fig. S5).

Over all, superhydrophilic stripes on hydrophilic patterned SLIPS promoted the rapid shedding of condensate droplets, and for fog harvest, hydrophilic lubricants were better than hydrophobic lubricants. In addition, the arrangement of superhydrophilic stripes also affected fog harvest efficiency. The results showed that arrays of superhydrophilic stripes with a spacing of 0.6 mm brought the greatest synergistic changes to the growth and separation of condensate droplets. The fog harvest efficiency of SSP0.6 was $160.38 \text{ mg}\cdot\text{h}^{-1}\cdot\text{cm}^{-2}$, which was 27% higher than that of homogeneous hydrophilic SLIPS ($126 \text{ mg}\cdot\text{h}^{-1}\cdot\text{cm}^{-2}$), and higher than $98.94 \text{ mg}\cdot\text{h}^{-1}\cdot\text{cm}^{-2}$ from Yang's work (where the degree of supercooling was 20°C , and the relative humidity was 85%), and higher than $91.06 \text{ mg}\cdot\text{h}^{-1}\cdot\text{cm}^{-2}$ from Liu's work (where the degree of supercooling was 22°C , and the relative humidity was 70%). [50,51].

4. Conclusion

In summary, the hydrophilic patterned SLIPS with superhydrophilic stripes were created using a simple pulsed UV laser processing technique to achieve directional droplet transport and rapid fog harvest by combining the slippery property of the peristome of *Nepenthes* and hydrophilic patterns inspired by Desert beetle. Droplet behavior on the hydrophilic patterned SLIPS with a single superhydrophilic stripe and stripe array was investigated in experiments. Results showed that static contact angle and dynamic sliding angle on the surface were significantly anisotropic which is ascribed to the surface tension-induced large energy barrier in the direction perpendicular to the stripes and low sliding viscous force along the stripes. Therein, the sliding anisotropy of the droplet was related to the type of lubricant as well as the width and spacing of the hydrophilic stripe. The droplet can slide accurately along the designed S-shaped hydrophilic pattern on an inclined surface by taking advantage of sliding anisotropy. In addition, it was found that the fog harvest rate was enhanced on hydrophilic patterned SLIPS compared with superhydrophobic surfaces and homogeneous SLIPS due to the low sliding resistance of condensate on SLIPS, efficient condensate transferring from SLIPS to superhydrophilic stripes and liquid shedding along the stripes for departing.

This simple and efficient UV laser processing technique used to fabricate functional surfaces can be extended to different substrates. In addition, the hydrophilic patterned SLIPS proposed in this work have potential applications, such as lab-on-a-chip devices and the energy harvesting field.

CRedit authorship contribution statement

X.Y. proposed the initial idea; B.Q. and X.Y. designed the experiment and analyzed the results; B.Q. fabricated the hydrophilic patterned SLIPS samples and characterized the droplet dynamic behavior. X.W. supervised the project and provided critical suggestions. B.Q. and X.Y. drafted the manuscript and all authors revised the manuscript.

Declaration of Competing Interest

The authors declare that they have no known competing financial interests or personal relationships that could have appeared to influence the work reported in this paper.

Acknowledgements

This research was financially supported by the National Natural Science Foundation of China (NSFC, 51905267), the Natural Science Foundation of Jiangsu Province (BK20190411), the China Postdoctoral Science Foundation (2020TQ0148) and Fundamental Research Funds for the Central Universities (NT2020011).

Appendix A. Supporting information

Supplementary data associated with this article can be found in the online version at doi:10.1016/j.colsurfa.2022.128398.

References

- [1] M. Cheng, M. Song, H. Dong, F. Shi, Surface adhesive forces: a metric describing the drag-reducing effects of superhydrophobic coatings, *Small* 11 (2015) 1665–1671.
- [2] L. Wang, Q. Gong, S. Zhan, L. Jiang, Y. Zheng, Robust anti-icing performance of a flexible superhydrophobic surface, *Adv. Mater.* 28 (2016) 7729–7735.
- [3] J. Sun, C. Wang, J. Song, L. Huang, Y. Sun, Z. Liu, C. Zhao, Y. Li, Multi-functional application of oil-infused slippery Al surface: from anti-icing to corrosion resistance, *J. Mater. Sci.* 53 (2018) 16099–16109.
- [4] W.-T. Cao, Y.-J. Liu, M.-G. Ma, J.-F. Zhu, Facile preparation of robust and superhydrophobic materials for self-cleaning and oil/water separation, *Colloid Surf. A* 529 (2017) 18–25.
- [5] X. Li, Z. Gao, B. Li, X. Zhang, Y. Li, J. Sun, Self-healing superhydrophobic conductive coatings for self-cleaning and humidity-insensitive hydrogen sensors, *Chem. Eng. J.* 410 (2021), 128353.
- [6] T. Wu, W.-h Xu, K. Guo, H. Xie, J.-p Qu, Efficient fabrication of lightweight polyethylene foam with robust and durable superhydrophobicity for self-cleaning and anti-icing applications, *Chem. Eng. J.* 407 (2021), 127100.
- [7] Z. Zheng, C. Liao, Y. Xia, W. Chai, C. Xie, W. Zhang, Y. Liu, Facile fabrication of robust, biomimetic and superhydrophobic polymer/graphene-based coatings with self-cleaning, oil-water separation, anti-icing and corrosion resistance properties, *Colloid Surf. A* 627 (2021), 127164.
- [8] N.J. Cira, A. Benusiglio, M. Prakash, Vapour-mediated sensing and motility in two-component droplets, *Nature* 519 (2015) 446–450.
- [9] A.A. Popova, S.M. Schillo, K. Demir, E. Ueda, A. Nesterov-Mueller, P.A. Levkin, Droplet-array (DA) sandwich chip: a versatile platform for high-throughput cell screening based on superhydrophobic-superhydrophilic micropatterning, *Adv. Mater.* 27 (2015) 5217–5222.
- [10] Y. Tang, X. Yang, Y. Li, D. Zhu, Design of hybrid superwetting surfaces with self-driven droplet transport feature for enhanced condensation, *Adv. Mater. Interfaces* 8 (2021), 2100284.
- [11] K. Ichimura, S.K. Oh, M. Nakagawa, Light-driven motion of liquids on a photoresponsive surface, *Science* 288 (2000) 1624–1626.
- [12] C. Li, R. Guo, X. Jiang, S. Hu, L. Li, X. Cao, H. Yang, Y. Song, Y. Ma, L. Jiang, Reversible switching of water-droplet mobility on a superhydrophobic surface based on a phase transition of a side-chain liquid-crystal polymer, *Adv. Mater.* 21 (2009) 4254–4258.
- [13] S. An, M. Zhu, K. Gu, M. Jiang, Q. Shen, B. Fu, C. Song, P. Tao, T. Deng, W. Shang, Light-driven motion of water droplets with directional control on nanostructured surfaces, *Nanoscale* 12 (2020) 4295–4301.
- [14] X. Yang, X. Liu, Y. Lu, J. Song, S. Huang, S. Zhou, Z. Jin, W. Xu, Controllable water adhesion and anisotropic sliding on patterned superhydrophobic surface for droplet manipulation, *J. Phys. Chem. C* 120 (2016) 7233–7240.
- [15] M. Tenjimabayashi, M. Higashi, T. Yamazaki, I. Takenaka, T. Matsubayashi, T. Moriya, M. Komine, R. Yoshikawa, K. Manabe, S. Shiratori, Droplet motion control on dynamically hydrophobic patterned surfaces as multifunctional liquid manipulators, *ACS Appl. Mater. Interfaces* 9 (2017) 10371–10377.
- [16] K. Hou, X. Li, Q. Li, X. Chen, Tunable wetting patterns on superhydrophilic/superhydrophobic hybrid surfaces for enhanced dew-harvesting efficacy, *Adv. Mater. Interfaces* 7 (2019), 1901683.
- [17] R. Ledesma-Aguilar, R. Nistal, A. Hernández-Machado, I. Pagonabarraga, Controlled drop emission by wetting properties in driven liquid filaments, *Nat. Mater.* 10 (2011) 367–371.
- [18] Y. Tang, X. Yang, Y. Li, Y. Lu, D. Zhu, Robust micro-nanostructured superhydrophobic surfaces for long-term dropwise condensation, *Nano Lett.* 21 (2021) 9824–9833.
- [19] X. Dai, N. Sun, S.O. Nielsen, B.B. Stogin, J. Wang, S. Yang, T.-S. Wong, Hydrophilic directional slippery rough surfaces for water harvesting, *Sci. Adv.* 4 (2018) eaq0919.
- [20] K.A. Wier, T.J. McCarthy, Condensation on ultrahydrophobic surfaces and its effect on droplet mobility: ultrahydrophobic surfaces are not always water repellent, *Langmuir* 22 (2006) 2433–2436.
- [21] Y.-T. Cheng, D.E. Rodak, Is the lotus leaf superhydrophobic? *Appl. Phys. Lett.* 86 (2005), 144101.
- [22] T.S. Wong, S.H. Kang, S.K. Tang, E.J. Smythe, B.D. Hatton, A. Grinthal, J. Aizenberg, Bioinspired self-repairing slippery surfaces with pressure-stable omniphobicity, *Nature* 477 (2011) 443–447.

- [23] N. Wang, D. Xiong, Y. Lu, S. Pan, K. Wang, Y. Deng, Y. Shi, Design and fabrication of the lyophobic slippery surface and its application in anti-icing, *J. Phys. Chem. C* 120 (2016) 11054–11059.
- [24] S. Zouaghi, T. Six, S. Bellayer, S. Moradi, S.G. Hatzikiriakos, T. Dargent, V. Thomy, Y. Coffinier, C. Andre, G. Delaplace, M. Jimenez, Antifouling biomimetic liquid-infused stainless steel: application to dairy industrial processing, *ACS Appl. Mater. Interfaces* 9 (2017) 26565–26573.
- [25] C. Stamatopoulos, J. Hemrle, D. Wang, D. Poulidakos, Exceptional anti-icing performance of self-impregnating slippery surfaces, *ACS Appl. Mater. Interfaces* 9 (2017) 10233–10242.
- [26] C. Wei, G. Zhang, Q. Zhang, X. Zhan, F. Chen, Silicone oil-infused slippery surfaces based on sol-gel process-induced nanocomposite coatings: a facile approach to highly stable bioinspired surface for biofouling resistance, *ACS Appl. Mater. Interfaces* 8 (8) (2016) 34810–34819.
- [27] S. Anand, A.T. Paxson, R. Dhiman, J.D. Smith, K.K. Varanasi, Enhanced condensation on lubricant-impregnated nanotextured surfaces, *ACS Nano* 6 (2012) 10122–10129.
- [28] P. Wang, T. Li, D. Zhang, Fabrication of non-wetting surfaces on zinc surface as corrosion barrier, *Corros. Sci.* 128 (2017) 110–119.
- [29] Y. Liang, C. Li, P. Wang, D. Zhang, Fabrication of a robust slippery liquid infused porous surface on Q235 carbon steel for inhibiting microbiologically influenced corrosion, *Colloid Surf. A* 631 (2021), 127696.
- [30] P. Wang, D. Zhang, S. Sun, T. Li, Y. Sun, Fabrication of slippery lubricant-infused porous surface with high underwater transparency for the control of marine biofouling, *ACS Appl. Mater. Interfaces* 9 (2017) 972–982.
- [31] S. Sunny, N. Vogel, C. Howell, T.L. Vu, J. Aizenberg, Lubricant-Infused nanoparticulate coatings assembled by layer-by-layer deposition, *Adv. Funct. Mater.* 24 (2014) 6658–6667.
- [32] X. Yang, K. Zhuang, Y. Lu, X. Wang, Creation of topological ultraslippery surfaces for droplet motion control, *ACS Nano* 15 (2021) 2589–2599.
- [33] K.C. Park, P. Kim, A. Grinthal, N. He, D. Fox, J.C. Weaver, J. Aizenberg, Condensation on slippery asymmetric bumps, *Nature* 531 (2016) 78–82.
- [34] S. Ling, Y. Luo, L. Luan, Z. Wang, T. Wu, Inkjet printing of patterned ultra-slippery surfaces for planar droplet manipulation, *Sen. Actuator B-Chem.* 235 (2016) 732–738.
- [35] C. Zhang, B. Zhang, H. Ma, Z. Li, X. Xiao, Y. Zhang, X. Cui, C. Yu, M. Cao, L. Jiang, Bioinspired pressure-tolerant asymmetric slippery surface for continuous self-transport of gas bubbles in aqueous environment, *ACS Nano* 12 (2018) 2048–2055.
- [36] É. Ruiz-Gutiérrez, J.H. Guan, B. Xu, G. McHale, G.G. Wells, R. Ledesma-Aguilar, Energy invariance in capillary systems, *Phys. Rev. Lett.* 118 (2017), 218003.
- [37] J. Hui Guan, É. Ruiz-Gutiérrez, B.B. Xu, D. Wood, G. McHale, R. Ledesma-Aguilar, G. George Wells, Drop transport and positioning on lubricant-impregnated surfaces, *Soft Matter* 13 (2017) 3404–3410.
- [38] K. Zhuang, Y. Lu, X. Wang, X. Yang, Architecture-driven fast droplet transport without mass loss, *Langmuir* 37 (2021) 12519–12528.
- [39] M. Sharma, S. Gupta, B. Bhatt, G. Bhatt, S. Bhattacharya, K. Khare, Anisotropic motion of aqueous drops on lubricated chemically heterogeneous slippery surfaces, *Adv. Mater. Interfaces* 8 (2021), 2001916.
- [40] K. Maji, A. Das, M. Dhar, U. Manna, Synergistic chemical patterns on a hydrophilic slippery liquid infused porous surface (SLIPS) for water harvesting applications, *J. Mater. Chem. A* 8 (2020) 25040–25046.
- [41] H. He, C. Wang, X. Zhang, X. Ning, L. Sun, Facile fabrication of multi-scale microgroove textures on Ti-based surface by coupling the re-solidification bulges derived from nanosecond laser irradiation, *Surf. Coat. Technol.* 386 (2020), 125460.
- [42] B. Balu, A.D. Berry, D.W. Hess, V. Breedveld, Patterning of superhydrophobic paper to control the mobility of micro-liter drops for two-dimensional lab-on-paper applications, *Lab Chip* 9 (2009) 3066–3075.
- [43] C.G.L. Furmidge, Studies at phase interfaces. I. The sliding of liquid drops on solid surfaces and a theory for spray retention, *J. Colloid Sci.* 17 (1962) 309–324.
- [44] D.A. Olsen, P.A. Joyner, M.D. Olson, The sliding of liquid drops on solid surfaces, *J. Phys. Chem.* 66 (1962) 883–886.
- [45] A. Alizadeh, V. Bahadur, A. Kulkarni, M. Yamada, J.A. Ruud, Hydrophobic surfaces for control and enhancement of water phase transitions, *MRS Bull.* 38 (2013) 407–411.
- [46] S. Daniel, M.K. Chaudhury, J.C. Chen, Fast drop movements resulting from the phase change on a gradient surface, *Science* 291 (2001) 633–636.
- [47] C.M. Yadav A., Water desalination system using solar heat: a review, *Renew. Sustain. Energy Rev.* 67 (2017) 1308–1330.
- [48] A.D. Khawaji, I.K. Kutubkhanah, J.-M. Wie, Advances in seawater desalination technologies, *Desalination* 221 (2008) 47–69.
- [49] A.R. Parker, C.R. Lawrence, Water capture by a desert beetle, *Nature* 414 (2001) 33–34.
- [50] K.-S. Yang, Y.-Y. Huang, Y.-H. Liu, S.-K. Wu, C.-C. Wang, Enhanced dehumidification via hybrid hydrophilic/hydrophobic morphology having wedge gradient and drainage channels, *Heat. Mass Transf.* 55 (2019) 3359–3368.
- [51] W. Liu, P. Fan, M. Cai, X. Luo, C. Chen, R. Pan, H. Zhang, M. Zhong, An integrative bioinspired venation network with ultra-contrasting wettability for large-scale strongly self-driven and efficient water collection, *Nanoscale* 11 (2019) 8940–8949.